Seismic behavior of slab-column connections with varying flexural reinforcement ratio

Mariana Rossi[1], Brisid Isufi [1,*], António Pinho Ramos [1, 2]

1. NOVA School of Science & Technology, UNL, Caparica, Portugal
2. CERIS, Lisbon, Portugal

[*]Corresponding author email: b.isufi@campus.fct.unl.pt

Abstract

This paper presents the results of three flat slab specimens with varying flexural reinforcement ratio tested under constant gravity load and reversed horizontal cyclic loading. The tests are a continuation of the experimental work conducted at FCT/UNL during the last years on specimens with the same overall geometry (4.15 × 1.85 × 0.15 m^3) and test setup. In contrast to past tests, in which all the specimens were reinforced with a nearly 1% flexural reinforcement ratio, the new specimens presented herein have a flexural reinforcement ratio varying from 0.64% (two specimens) to 1.34% (one specimen). One of the specimens with low flexural reinforcement ratio was also reinforced with headed studs whereas the other two specimens had no punching shear reinforcement. The magnitude of the gravity loads was chosen such that the ratio between the gravity load and the concentric punching shear resistance remained comparable to that of previously tested specimens at FCT/UNL: around 50%. It is shown that the presence of headed studs leads to a significant improvement of the displacement capacity of slab-column connections, as it was previously observed in tests on specimens with 1% flexural reinforcement ratio. The drift capacity of specimens without punching shear reinforcement was significantly lower.

Keywords: *Cyclic loading; seismic behavior; flat slab; punching; flexural reinforcement.*

1. Introduction

Flat slab frames are popular gravity load resisting systems in reinforced concrete buildings. The slab – column connections must be able to carry the gravity loads without a punching shear failure under the displacements imposed by the primary seismic system during an earthquake. However, the behavior of slab – column connections under combined gravity and lateral loading is not entirely understood and covered by the design codes (for example, Eurocode 8 (CEN, 2004b)).

For slabs under gravity loads, it has been shown by numerous studies that the amount of flexural reinforcement influences the behavior and failure modes (Ghali and Gayed, 2019; Guandalini, Burdet, and Muttoni, 2009; Muttoni, 2008; Torabian *et al.*, 2019). As the amount of flexural reinforcement is decreased, the load carrying capacity of the slab is governed by flexure rather than punching shear. In slabs with low reinforcement ratios, the flexural reinforcement yields and the slab behaves in a ductile manner until punching occurs as a function of the opening of the critical shear crack (Muttoni, 2008) at relatively large displacements (for example, refer to examples in Torabian *et al.* (2019; 2020)).

For lateral loading, such as during an earthquake, the behavior is more complex. However, it can be expected a significant influence of the flexural reinforcement ratio in the maximum unbalanced moment transfer capacity of the slab. On the other hand, the increased unbalanced moment capacity due to flexure can result in a punching shear failure due to the increase of stresses in the vicinity of the column.

The influence of flexural reinforcement on the seismic behavior of slab – column connections has been studied experimentally in the past by various authors (Drakatos, Muttoni, and Beyer, 2016; Hawkins, Mitchell, and Sheu, 1974; Morrison, Hirasawa, and Sozen, 1983; Robertson and Johnson, 2006; Symonds, Mitchell, and Hawkins, 1976; Tian *et al.*, 2008). The tests in the 1970s showed that the amount of flexural reinforcement and its layout (concentrated near the column or distributed) are among

the most important factors determining the seismic response of a slab – column connection under lateral loading.

Among the specimens tested by Morrison *et al.* (1983), the flexural reinforcement ratio was the experimental variable (three ratios 0.65%, 0.98% and 1.31% respectively were tested). These three specimens were tested without gravity load. The response was dominated by flexure and no punching occurred in these specimens. Among the six 114 mm thick specimens reported in Robertson and Johnson (2006), four differed by the amount of top flexural reinforcement ratio (0.39%, 0.53% and 0.93% over column width + 3 times slab thickness) and layout. The results of Robertson and Johnson (2006) showed that the increase of the flexural reinforcement ratio can increase the horizontal load (unbalanced moment) capacity, but the deformation capacity can be hindered by punching shear failure. Tian *et al.* (2008) showed that the punching shear capacity and lateral stiffness were both increased with the increase of the flexural reinforcement ratio.

Drakatos *et al.* (2016) tested 13 specimens without punching shear reinforcement and thickness of 250 mm. The experimental variables were the loading history (monotonic versus reversed cyclic), gravity load and the flexural reinforcement ratio (two levels, around 0.8% and 1.6%). Drakatos *et al.* (2016) showed that cyclic loading affects slabs with lower flexural reinforcement ratio more than slabs with high flexural reinforcement ratio. Also, they showed that increasing the reinforcement ratio increases the lateral stiffness of the slab – column connections, but the influence of the flexural reinforcement ratio on the unbalanced moment capacity and deformation capacity depended heavily on the applied gravity load.

The present work takes advantage of a series of tests conducted in the past at NOVA School of Science & Technology on specimens with the same geometry and flexural reinforcement ratio approximately 1% and adds the flexural reinforcement ratio as an experimental variable. All the tests published in Almeida *et al.* (2016) (on specimens without punching shear reinforcement), Isufi *et al.* (2019; 2020) (specimens with headed studs), Almeida *et al.* (2020; 2020) (specimens with stirrups and post-installed bolts) as well as tests reported in Gouveia *et al.* (2019); Inácio *et al.*, (2020) (high strength concrete and fiber reinforced concrete) had the same geometry, approximate gravity load relative to the punching shear resistance, and the same flexural reinforcement detailing. The new tests presented herein contribute to enlarging the database of tests conducted for the purpose of studying the influence of flexural reinforcement in the seismic behavior of slab – column connections. Additionally, the tests pave the way for additional insight based on comparisons with the large number of tests conducted in the past at FCT/UNL under similar conditions but with a fixed value of the flexural reinforcement ratio (1%).

2. Experimental program

2.1. Specimens

Three specimens with overall dimensions of 4.15 × 1.85 m^2 and thickness 0.15 m were tested. The slabs were designed in an attempt to represent an interior slab-column connection of an office building at 2/3 scale and centered to the specimens, connected to a steel column with a square base section 0.25 × 0.25 m^2 and total height of 2.0 m, with 1.0 m above and below the slab. Longitudinal and shear reinforcement was designed taking into account the experimental campaigns previously developed by Isufi *et al.* (2019) and Almeida *et al*. (2016).

The specimens differed in longitudinal and shear reinforcement: slabs C-Ref-L and C-SSR5-L had the same longitudinal reinforcement ratio of ρ=0.64% but 5 perimeters of studs were installed to C-SSR5-L as punching shear reinforcement. For the top reinforcement, ø12mm bars were placed near the column and ø10mm bars outside the column region in these two specimens. Bottom reinforcement consisted of ø10mm bars. Reinforcing bar placement details for these two specimens (C-Ref-L and C-SSR5-L) are displayed in Figure 1a.

Shear reinforcement installed in C-SSR5-L consisted in five rows of three studs in each side of the column. The top of the studs was connected by rectangular steel bars of 25 × 8 mm^2 for anchorage and to ensure the correct spacing between bars, whereas the bottom of each stud was welded to a 25 × 25 mm^2 bar (Figure 2b). The headed studs were positioned as shown in Figure 2c and twenty-five strain gauges were installed in different studs to obtain strain data during the test.

The other specimen (C-Ref-H) was designed with a higher longitudinal ratio, ρ=1.34%, and no punching shear reinforcement. Bars with ø12mm spaced at 100mm composed the bottom reinforcement in both directions and ø12mm bars were used in the column region with ø10mm bars further from the column. Details are shown in Figure 1b.

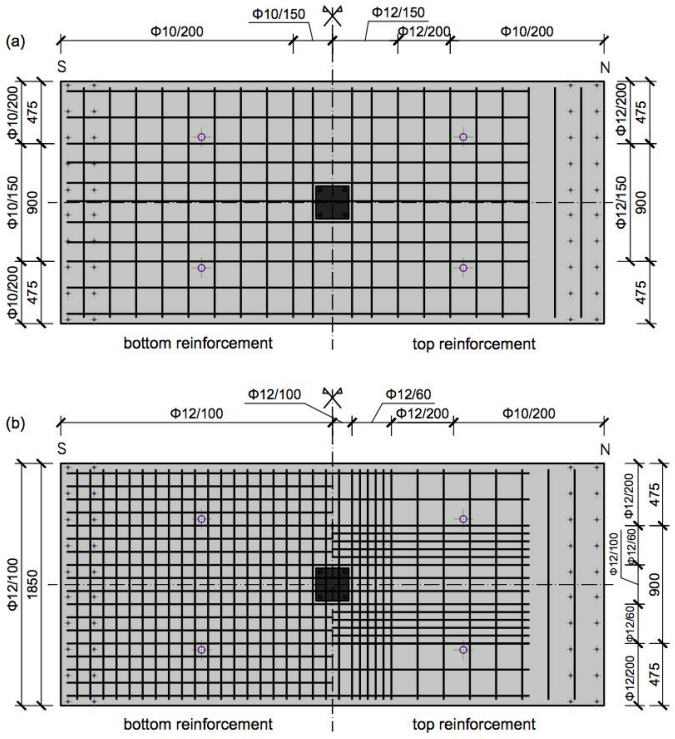

Figure 1. Top and Bottom Reinforcement: (a) C-Ref-L and C-SSR5-L; (b) C-Ref-H.

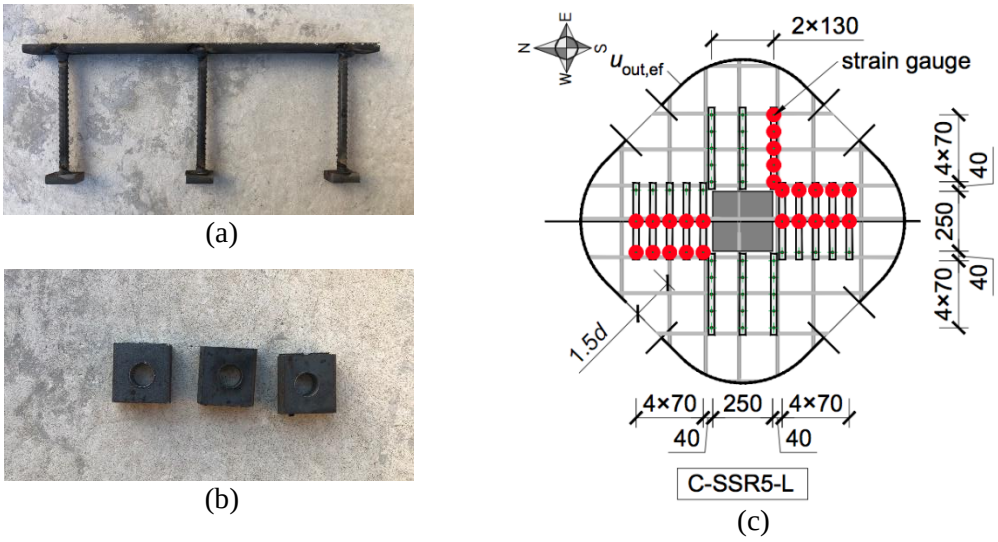

Figure 2. Headed Studs shear reinforcement details and positioning: a) a stud rail; b) bottom heads; c) layout.

Concrete samples were tested for all specimens after casting to acquire information for the concrete strength. The average values obtained for the concrete properties are summarized in Table 1, with f_c being the average cylinder strength and $f_{c,cube}$ the average cube strength.

For all three specimens the nominal concrete cover was 20 mm, but before casting the effective depth was measured in both directions in order to obtain the average values, d, displayed in Table 1. The same table displays the total gravity load (V_g), including the test setup weight and self-weight of the slab, and also the Gravity Shear Ratio (GSR) obtained as the ratio of V_g/V_0, in which V_0 is the shear resistance

without punching shear reinforcement, calculated based on Eurocode 2 (CEN, 2004a) but without partial factors of safety as shown in Eq. (1).

$$V_0 = 0{,}18k(100\rho f_c)^{1/3}ud \quad (1)$$

where $k = 1 + \sqrt{\frac{200}{d}} \leq 2$, ρ is the longitudinal reinforcement ratio, f_c is the concrete strength, u is the control perimeter distanced $2d$ from the column and d is the average effective depth.

Table 1. Specimens details.

Specimen	d (mm)	f_c (MPa)	$f_{c,cube}$ (MPa)	V_0 (kN)	V_g (kN)	GSR (%)
C-Ref-L	117.30	31.27	2.79	284.17	165.23	58.1%
C-SSR5-L	117.16	46.61	3.37	324.16	181.53	56.0%
C-Ref-H	117.73	41.06	3.33	399.30	219.10	54.9%

2.2. Test setup and instrumentation

The experimental campaign was conducted at the Heavy Structures Laboratory at FCT/UNL with a test setup previously developed by Almeida *et al.* (2016). The test setup was designed to overcome some limitations of earlier works regarding boundary conditions. The setup at FCT/UNL allows vertical displacements at the edges of the specimens, equal bending moments and shear forces at opposite N-S edges, equal magnitude shear forces, mobility of the line of inflection along the longitudinal direction, resembling continuous flat slabs in the N-S direction. Furthermore, the setup enables the application of high vertical load ratios. For detailed descriptions of the test setup the reader is referred to Almeida et al. (2016); Ramos *et al.* (2017). An elevation view of the test setup is shown in Figure 3a and a photo is shown in Figure 3b.

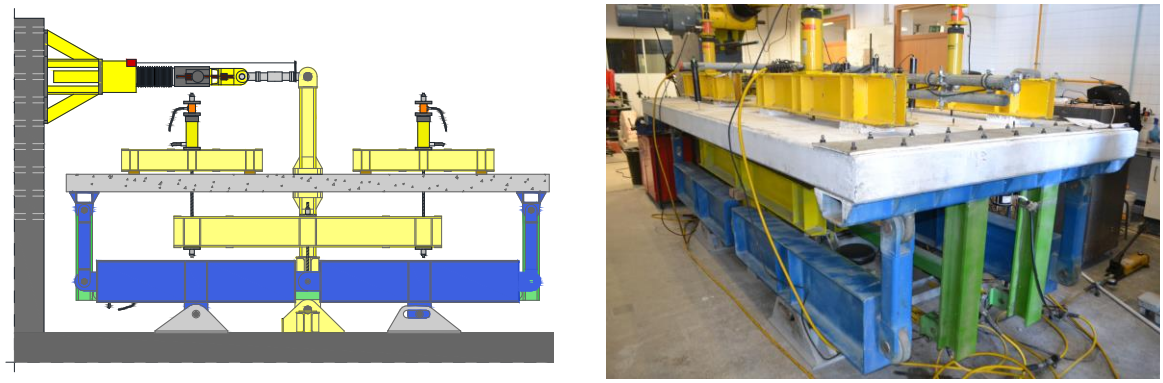

(a) (b)

Figure 3. Test setup: a) elevation view; b) photo.

Eight load points were distributed over the top surface of the specimens in order to apply the gravity load. Every two points were connected to a steel beam which was connected to a hydraulic jack and a load cell to control the applied load. To impose horizontal displacements, the top edge of the column was connected to a mechanical actuator fixed to the reaction wall and the horizontal displacements were measured by a displacement transducer attached to the actuator. The lower end of the column was pinned to the laboratory strong floor.

Fourteen displacements transducers were installed along the N-S and four along the E-W center lines to obtain the vertical displacements (deflections) throughout the test. The test protocol applied to all three specimens was the same as used in previous tests, consisting in first applying the vertical load until the target value (V_g in Table 1) was reached, which was then kept constant throughout the entire experiment, and then applying cyclic horizontal displacements with three cycle repetitions for drift ratios under 3.5%, two cycles for a 4.0% drift and only one for the following displacements until 6.0%.

3. Results

3.1. Test results

During the application of gravity load to C-Ref-L some small flexural cracks appeared in the column region and with the beginning of horizontal displacements the existing cracks grew wider and further from the column and new cracks could be noticed in the positive moment region. For the 1.0% cycles new cracks emerged for both positive and negative moments and the concrete cover on the column region started to deteriorate. During the first reversed cycle of the 1.5% drift ratio the specimen failed with a sudden decrease of the horizontal load and brittle punching failure before completing a full cycle.

Similarly, thin flexural cracks emerged near the column of C-SSR5-L with the application of the vertical load. When horizontal displacements started to be imposed existing cracks showed a width and length increase and positive bending moments cracks also started to emerge. As higher drifts were applied all existing cracks presented a growth, but also new ones were noted. At a 2.5% drift ratio some cracks on the bottom side of the slab appeared near the column and also some damage to the concrete cover on both top and bottom surface of the slab was observed. At 6% drift, the specimen was severely cracked and deformed. However, the specimen did not reach failure and the test was stopped at a 6.0% drift ratio due to test setup limitations.

During testing of C-Ref-H, small flexural cracks near the column and in positive bending moment regions emerged with the application of the vertical load. For 0.5% drift ratio, the existing cracks opened more and developed further from the column, as also new cracks appeared on the upper and lower side of the specimen. During 1.0% drift ratios new cracks emerged whereas the existing ones grew in length and thickness and damage to the concrete cover near the column was evident since the first cycle. The specimen failed during the last cycle of the 1.0% drift with a brittle punching shear failure.

3.2. Force – displacement relationships

The force – displacement (and unbalanced moment – drift) relationships are shown in Figure 4 for all three specimens. Note that a different scale of the axes is used in C-SSR5-L for clarity. Figure 4 shows a remarkable difference in the behavior of specimen C-Ref-L and the similar specimen C-SSR5-L but with shear reinforcement. While C-Ref-L failed before completing a full 1.5% drift cycle, specimen C-SSR5-L had a stable response with significant post-elastic yielding in the force – displacement relationship until the end of the test after 6% drift.

The behavior of C-SSR5-L was similar to that of specimens previously tested in Isufi *et al.* (2019) with headed studs shear reinforcement and higher flexural reinforcement ratio (approximately 1%), except that the yielding plateau in Figure 4 corresponds to a lower horizontal force (unbalanced moment) compared to the counterpart specimens in Isufi *et al.* (2019).

Comparing the two specimens without punching shear reinforcement (Figure 4) it is observed that the ultimate drift capacities were comparable: while C-Ref-H failed at 1% drift, specimen C-Ref-L failed during the first excursion towards negative 1.5% drift, without being able to complete a full cycle at 1.5% drift. It is noticeable from Figure 4 that the behavior of C-Ref-H with higher flexural reinforcement ratio and higher gravity load deteriorated earlier, even though the ratio V_g/V_0 was almost the same for both specimens (Table 1). This observation indicates that in addition to GSR (the ratio V_g/V_0), flexural capacity influences the response under lateral loading as well.

Two previously tested similar specimens with intermediate flexural reinforcement ratio (approximately 1%) failed at 1.0% drift (specimen C-50 in (Almeida *et al*., 2016) and specimen C-Ref in (Isufi *et al.*, 2019)) and exhibited a behavior that fits between that of C-Ref-L and C-Ref-H.

Table 2 summarizes the maximum horizontal force applied to the top of the column and the respective unbalanced moment (obtained by simply multiplying the horizontal force by the column total height) and the drift ratio corresponding to the maximum horizontal force. The maximum drift ratio attained by the specimen is also shown in Table 2.

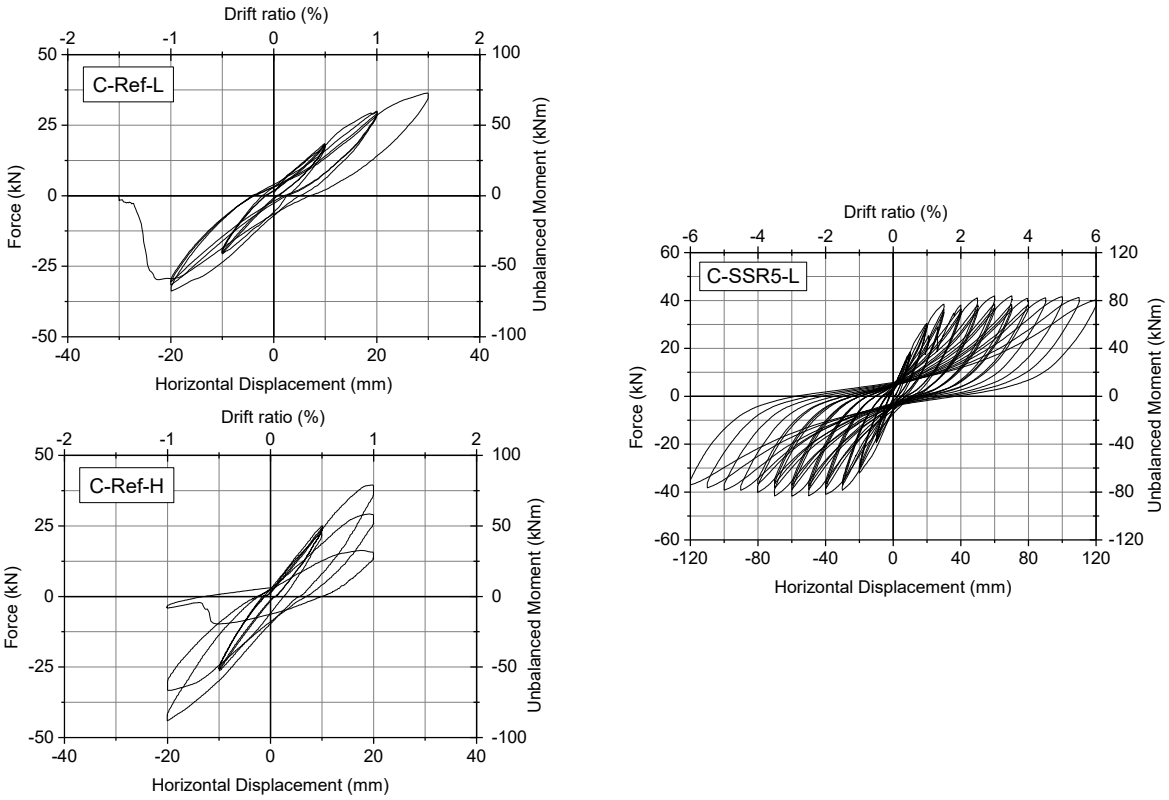

Figure 4. Force – displacement and unbalanced moment – drift relationships.

Table 2. Horizontal forces and failure drifts.

Specimen	Max. Horizontal Force (kN)	Max. Unbalanced Moment (kNm)	Drift at max. unbalanced moment	Maximum Drift
C-Ref-L	36.40	72.80	1.50%	1.50%
C-SSR5-L	41.92	83.84	3.00%	6.00%
C-Ref-H	44.08	88.16	-1.00%	1.00%

3.3. Deflections

The deflections obtained by the displacement transducers for the first cycle of each drift are displayed in Figure 5. Slab C-SSR5-L had the highest displacement for this first step, but the vertical load applied to this slab was higher than the one imposed to C-Ref-L. Even though the highest gravity load was for C-Ref-H, the higher longitudinal reinforcement ratio resulted on this slab suffering the smallest vertical displacement for gravity loading.

When horizontal displacements were imposed, the deflections increased due to the stiffness loss caused by the cyclic loading and unbalanced moments. Due to the gravity loading phase, C-SSR5-L started with larger displacements than C-Ref-L but this difference was reduced with bigger drifts and the differences between the two specimens until failure of C-Ref-L were small. For C-Ref-H, with higher flexural reinforcement ratio, the displacement increase for consecutive cycles was smaller compared to that of the other specimens.

Although specimen C-Ref-H had lower deflections, it failed during a lower drift ratio than the other specimens, as seen in Table 2, with a brittle failure.

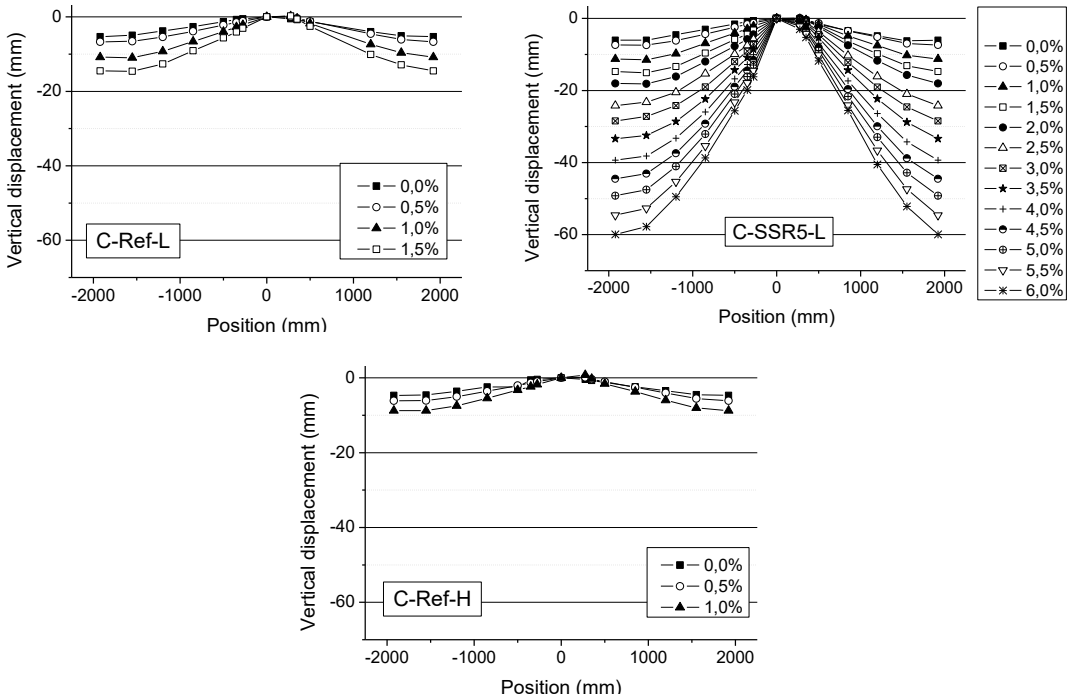

Figure 5. Deflection profiles along N-S direction.

4. Conclusions

The combined vertical and reversed horizontal cyclic loading tests of three slab – column specimens were briefly described. The purpose of the tests was to study the influence of slab's flexural reinforcement ratio in the seismic behavior of slab – column connections. One of the specimens, with flexural reinforcement ratio 0.64%, was reinforced with headed studs against punching shear failure whereas the other two specimens, one with flexural reinforcement ratio 0.64% and the other with 1.34% were without shear reinforcement.

In accordance with past experimental results, it was shown that the provision of headed studs can lead to a significant enhancement of the ultimate drift capacity under lateral loading. Punching failure was avoided in the specimen with headed studs shear reinforcement until the end of the test at 6% drift, which is well above drifts expected in practice for reinforced concrete buildings subjected to earthquakes. The specimens without shear reinforcement failed at drifts around 1%, similar to previously tested similar specimens with intermediate flexural reinforcement ratio (approximately 1%).

The specimens without shear reinforcement (including C-50 and C-Ref previously reported in the literature with intermediate reinforcement ratio) had approximate values of the gravity shear ratio (GSR) and they failed at comparable ultimate drifts (around 1% drift, with the exception of C-Ref-L which completed a half-cycle at 1.5% drift). However, it was shown that the seismic behavior deteriorated with the increase of the flexural reinforcement ratio, indicating that the flexural reinforcement influences the behavior of slab – column connections under seismic loading in addition to GSR.

Acknowledgements

This work received support from Fundação para a Ciência e Tecnologia – Ministério da Ciência, Tecnologia e Ensino Superior through project PTDC/ECI-EST/ 30511/2017. The authors wish to thank CONCREMAT for producing the specimens.

References

Almeida, A. F. O., Alcobia, B., Ornelas, M., Marreiros, R., and Ramos, A. P. (2020). Behaviour of reinforced-concrete flat slabs with stirrups under reversed horizontal cyclic loading. Magazine of Concrete Research, 72(7), 339–356. https://doi.org/10.1680/jmacr.18.00209

Almeida, A. F. O., Inácio, M. M. G., Lúcio, V. J. G., and Ramos, A. P. (2016). Punching behaviour of RC flat slabs under reversed horizontal cyclic loading. Engineering Structures, 117, 204–219. https://doi.org/10.1016/j.engstruct.2016.03.007

Almeida, A. F. O., Ramos, A. P., Lúcio, V., and Marreiros, R. (2020). Behavior of RC flat slabs with shear bolts under reversed horizontal cyclic loading. Structural Concrete, 21(2), 501–516. https://doi.org/10.1002/suco.201900128

CEN. (2004a). EN 1992-1-1. Eurocode 2 — Design of concrete structures. Part 1-1: General rules and rules for buildings.

CEN. (2004b). EN 1998-1. Eurocode 8: Design of structures for earthquake resistance - Part 1: General rules, seismic actions and rules for buildings.

Drakatos, I. S., Muttoni, A., and Beyer, K. (2016). Internal slab-column connections under monotonic and cyclic imposed rotations. Engineering Structures, 123, 501–516. https://doi.org/10.1016/j.engstruct.2016.05.038

Ghali, A., and Gayed, R. B. (2019). Universal Design for Punching Resistance of Concrete Slabs. ACI Structural Journal, 116(1), 207–212. https://doi.org/10.14359/51710866

Gouveia, N. D., Faria, D. M. V., and Ramos, A. P. (2019). Assessment of SFRC flat slab punching behaviour – part II: reversed horizontal cyclic loading. Magazine of Concrete Research, 71(1), 26–42. https://doi.org/10.1680/jmacr.17.00344

Guandalini, S., Burdet, O. L., and Muttoni, A. (2009). Punching tests of slabs with low reinforcement ratios. ACI Structural Journal, 106(1), 87–95. https://doi.org/10.14359/56287

Hawkins, N. M., Mitchell, D., and Sheu, M. S. (1974). Cyclic behavior of six reinforced concrete slab-column specimens transferring moment and shear. Seattle, Washington.

Inácio, M., Isufi, B., Lapi, M., and Ramos, A. P. (2020). Rational Use of High-Strength Concrete in Flat Slab-Column Connections under Seismic Loading. ACI Structural Journal, 117(6), 297–310. https://doi.org/10.14359/51728080

Isufi, B., Pinho Ramos, A., and Lúcio, V. (2019). Reversed horizontal cyclic loading tests of flat slab specimens with studs as shear reinforcement. Structural Concrete, 20(1), 330–347. https://doi.org/10.1002/suco.201800128

Isufi, B., Ramos, A. P., and Lúcio, V. (2020). Post-earthquake Performance of a Slab-Column Connection with Punching Shear Reinforcement. Journal of Earthquake Engineering, (in Press)(00), 1–23. https://doi.org/10.1080/13632469.2020.1713924

Morrison, D. G., Hirasawa, I., and Sozen, M. A. (1983). Lateral-Load Tests of R/C Slab-Column Connections. Journal of Structural Engineering, 109(11), 2698–2714. https://doi.org/10.1061/(ASCE)0733-9445(1983)109:11(2698)

Muttoni, A. (2008). Punching Shear Strength of Reinforced Concrete Slabs. ACI Structral Journal, 105(4), 440–450. https://doi.org/10.14359/19858

Ramos, A., Marreiros, R., Almeida, A., Isufi, B., and Inácio, M. (2017). Punching of flat slabs under reversed horizontal cyclic loading. In C. E. Ospina, D. Mitchell, and A. Muttoni (Eds.), ACI Special Publication (Vol. 315, pp. 253–272). ACI, *fib*.

Robertson, I., and Johnson, G. (2006). Cyclic lateral loading of nonductile slab-column connections. ACI Structural Journal, 103(3), 356–364. https://doi.org/10.14359/15313

Symonds, D. W., Mitchell, D., and Hawkins, N. M. (1976). Slab-column connections subjected to high intensity shears and transferring reversed moments. SM 76-2. Seattle, Washington.

Tian, Y., Jirsa, J. O., Bayrak, O., Widianto, and Argudo, J. F. (2008). Behavior of slab-column connections of existing flat-plate structures. ACI Structural Journal, 105(5), 561–569.

Torabian, A., Isufi, B., Mostofinejad, D., and Ramos, A. P. (2019). Behavior of thin lightly reinforced flat slabs under concentric loading. Engineering Structures, 196. https://doi.org/10.1016/j.engstruct.2019.109327

Torabian, Ala, Isufi, B., Mostofinejad, D., and Pinho Ramos, A. (2020). Flexural strengthening of flat slabs with FRP composites using EBR and EBROG methods. Engineering Structures, 211, 110483. https://doi.org/10.1016/j.engstruct.2020.110483